

**3D Visualization
of Pose Determination:
Application to SPECT Imaging**

by

R. Mullick and N.F. Ezquerra
College of Computing

E.V. Garcia, C.D. Cooke and R.D. Folks
Division of Nuclear Medicine
School of Medicine

GIT-GVU-93-28
July 1993

**Graphics, Visualization & Usability
Center**

Georgia Institute of Technology
Atlanta GA 30332-0280

3D Visualization of pose determination : Application to SPECT imaging

R. Mullick and N. F. Ezquerro*
Graphics, Visualization, and Usability Center
Department of Electrical Engineering
*College of Computing
Georgia Institute of Technology
Email : rakesh@cc.gatech.edu

E. V. Garcia, C. D. Cooke, and R.D. Folks
Division of Nuclear Medicine
School of Medicine
Emory University
Atlanta, GA 30322

ABSTRACT

Pose determination of 3D objects is a topic of active research, particularly in the area of medical imaging. The determination of the pose or orientation of a 3D object in a 3D dataset can be viewed as a two-fold problem : 1) The determination of the orientation of the object; and 2) the visualization of the object along with the determined orientation of the object. An attempt has been made to compute and visualize the orientation of left ventricle (LV) of the heart from SPECT data. A semi-automatic technique to first filter the acquired SPECT data and then compute the 3D orientation of the LV is under development. Volume visualization techniques have been employed to better visualize and comprehend the structure and orientation of the LV.

1. INTRODUCTION AND BACKGROUND

The natural pose of the heart seldom coincides with the transaxial (head-to-feet) direction defined by the coordinate systems of imaging scanners used in cardiovascular nuclear medicine. However, to make a diagnostic interpretation from these images, such as those obtained from single-photon emission computed tomography (SPECT), the orientation of the Left Ventricle (LV) must be determined. Knowledge of this LV orientation enables the appropriate slicing of tomographic data for defining the 3D myocardial perfusion distribution. Interpretation of this distribution, in turn, allows for assessing the extent and severity of coronary artery disease (CAD). At present, this arduous and time consuming task is performed by medical technicians and system operators. These experts "eyeball" the LV long-axis orientation by viewing the data from two perspectives. The result of this crude technique is two angles which represent the orientation of the LV as an offset from the "straight-up" position parallel to the X-axis [See Figure 1]. The operator first localizes the LV in one of the mid-ventricular transaxial slices and highlights the orientation of the LV in that view yielding the planar angle (α). The imaging system then re-slices the 3D data along that orientation allowing the operator to view the vertical-long slices in which the operator then indicates the angle of elevation (β) of the LV.

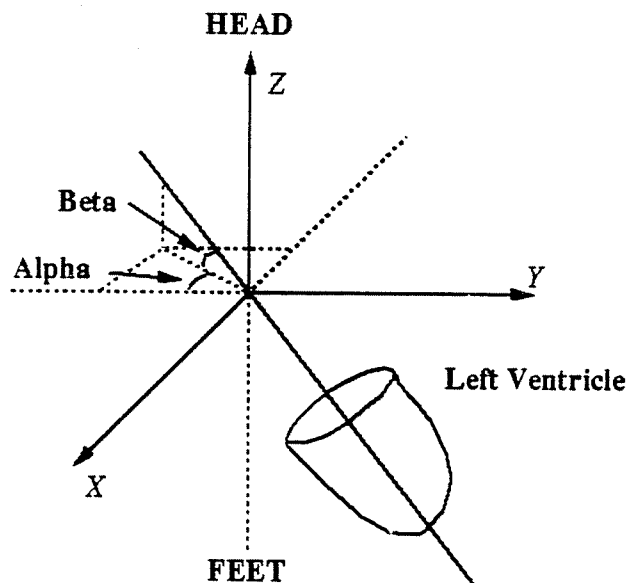


Figure 1. Geometric description of 3D pose determination

This technique is just one of the many ways nuclear medicine technicians determine the orientation of the LV and other organs to aid in diagnostic interpretation. These non-standardized techniques lead to inter- and intra-observer variability and thereby affect the consistency of the clinical diagnosis. Inter-observer agreement for the horizontal and the vertical angles have been shown¹ to range between 0.70-0.83. It has also been demonstrated² that if the LV long-axis is incorrectly identified in either the transaxial or sagittal geometry, the reconstructed orthogonal slices can be distorted. In many instances, the improper selection of the base and apex of the left-ventricle result in visible artifacts. Thus one can conclude^{1,2,3} that the manual selection of the LV long-axis has a number of inherent errors and limitations. As an attempt to overcome many of these deficiencies, a semi-automatic technique is presented here to determine the LV long axis and thereby determine and visualize the pose of the LV. This study emphasizes the importance of improved 3D visualization of the SPECT data for inferring the orientation of organs from volume data.

2. DATA CHARACTERISTICS AND PRELIMINARY CONSIDERATIONS

Inherent limitations of SPECT imaging yield a challenging problem. The specific aim in nuclear medicine, and in particular Tl^{201} and Tc^{99m} cardiac SPECT imagery is to study the physiology and not the structure of the imaged organ. However, it is desirable to infer structural (vascular) information from these images. Thus, the functional information can be misleading in terms of inferring the possibly affected coronaries. In turn, improper slicing (as well as hypoperfused regions in the data) can make the interpretive task increasingly difficult.

The constant "beating" of the heart has an additional blurring effect on this inherently low-resolution imaging modality. Current resolutions of such imaging systems range from 4 mm to 7 mm resulting in small sized 3D datasets. Thus small errors (≤ 1 voxel) in localization of extracted features can lead to considerable anomalies in the reported orientation of the LV. In addition, Compton scattering and other physical phenomena make the data quite noisy. Therefore, the data can be viewed as low-resolution, noisy, temporally integrated, and sparse. Therein lies the importance of proper pose determination, to minimize possible data loss and maximize the available data. A sample normal patient volume (3D) dataset in form of consecutive transaxial slices is presented in *Figure 2*.

3. RELATED RESEARCH

Most previous, related studies^{1,3,4} to address this issue have concentrated on mimicking the protocol used by the medical technicians and have yielded moderately favorable results. He et. al reorient the Left Ventricular Long Axis using the Linear Fitting Method¹. The linear activity profiles between the apical limits on a midventricular transaxial slice and the basal limits on a midventricular sagittal slice are plotted line by line. The activity distribution along each line is analyzed to determine the left ventricular long axis. This method does require an operator to first determine a midventricular slice in each view and then outline the apical and basal limits in the selected view. The reproducibility has been shown to be significantly better with this semi-automatic method than with the manual selection of the LV long axis. The authors have also noted that myocardial Tl^{201} uptake and myocardial thickening^{1,5} may also effect the definition of points with minimum counts and might hinder in the accurate determination of the LV long axis.

A similar model of the LV long axis, a 3D straight line, has been used by Cauvin et. al⁶ to reorient the myocardium in Tl^{201} SPECT. In their method they have modeled the left ventricle to be an ellipsoid. Blockland et. al⁷ have also suggested an ellipsoidal model for the LV. The raw data in form of transverse sections is *manually* preprocessed to center, zoom, and mask out areas outside the left ventricle. Three dimensional morphological techniques and least square fitting algorithms are then employed to determine the LV long axis. The results reported by Cauvin et. al are encouraging. It must be noted here that in that study, a manual stage is part of the process and that 64 raw transaxial slices were used for the analysis, instead of the usual 20-30 6 mm thick slices. Additionally, the LV was approximated to have an ellipsoidal shape, whereas volume visualization shows that the LV is shaped differently, as explained in the subsequent discussions.

4. METHODS

4.1 Pose Determination

The automatic determination of the orientation of the LV Long-Axis from SPECT data involves three main steps. Following data acquisition, the patient specific 3D dataset is processed using a set of image processing and computer vision techniques to segment and extract the left ventricle. This filtered 3D volume is then analyzed using volume visualization techniques to construct the 3D topology of the left ventricle. At this stage the structure of the left ventricle is represented by a collection of triangular polygons. This topological information is then scrutinized to determine the orientation of the LV. The final result of this three-step process is a 3D curve representing the long axis of the left ventricle. It should be stressed that the result is thus provided not as a straight line, but as a curve in 3D space that more closely represents the natural shape of the LV mass.

4.1.1 Data Acquisition

To generate the 3D dataset, patients are stressed using multistage treadmill exercise and a dose of 3.5 mCi of thallium-201 is injected at maximum exercise; the patient continues to exercise for 45 to 90 seconds after injection. At approximately six minutes, and again at three to six hours after injection of thallium-201, the patients are imaged using a rotating, large field-of-view scintillation camera tomographic unit. Thirty-two projections are obtained for a preset time (40 seconds each) in an arc of 180 degrees. Subsequently, each of the projections is corrected for non-uniformity, properly aligned, filtered, and smoothed to reconstruct the transverse axial tomograms, each ~ 6 mm thick, encompassing the entire heart [Same as Figure 2]. A more detailed description of the actual clinical protocol is described in previous publications.^{8,9,10,11}

4.1.2 Left Ventricle Segmentation and Extraction

A set of routines have been developed to extract the Left Ventricle voxels from the transaxial slice data. The process involves the determination of an optimal threshold to first filter out noise in the volume data. This preprocessing stage involves computation of the cumulative histogram of the volume data. The histogram is then fitted to a decaying exponential and the optimal threshold is determined to be the intensity value at which the amplitude of the histogram falls below 5% of its maximum value. Figure 3 presents the histogram of a representative 3D dataset, the corresponding fit to it, and the choice of the threshold. The validity of this threshold value is further analyzed and the value is iteratively incremented until the cavity in the LV is visible.

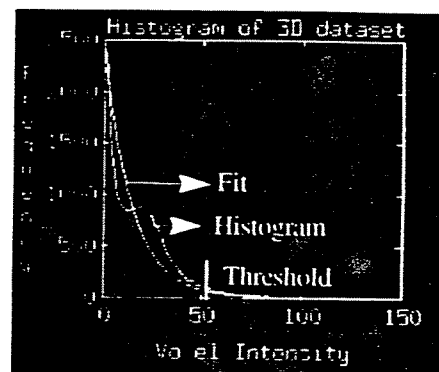


Figure 3.

This step is followed by the automatic determination of the mid-ventricular slice in the data. The presence of the right ventricle (RV) hinders the accurate determination of the LV long axis. This mid-ventricular slice [See Figure 4] is then used as a guide in the process to separate the Right Ventricle (RV) and the LV. The presence of the RV is removed using connected components labeling and region analysis of the transaxial dataset. The contents of each transaxial image are first processed using the morphological technique¹² of erosion using a 2×2 structuring element. The erosion process disconnects and thins out the walls of myocardium making it feasible to separate the two ventricles. Labeling technique is then employed to identify and mark each distinct mass in each image. All smaller masses except the largest one and those lying within a pre-determined region (based on analysis of the mid-ventricular slice) in each image are deleted. At this stage all remaining masses are taken to be part of the left ventricular myocardium. 3D connectivity of these 2D masses is also analyzed and the single largest connected mass in the 3D volume dataset is thus extracted. This concludes the filtering, segmentation, and feature extraction part of the orientation determination process.

4.1.3 Topology Construction and Model Creation

To construct the 3D topology of the myocardium, the Marching Cubes Algorithm^{13,14,15,16} was used. The iso-surface of the filtered 3D dataset at the optimal threshold value was computed using this algorithm. The marching cubes algorithm¹⁵ creates the iso-surface of a set of three-dimensional data by :

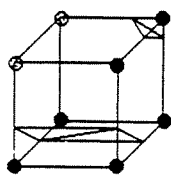


Figure 5. Illustration of choice of surface polygons in the Marching Cubes algorithm

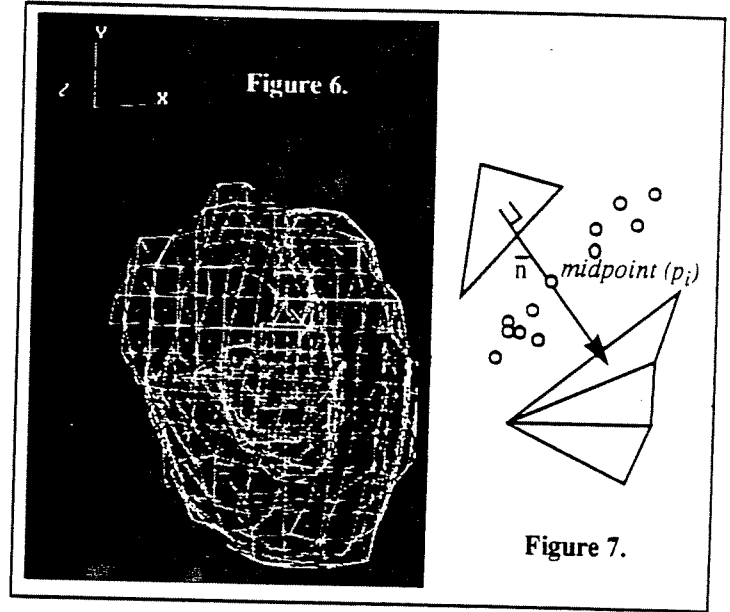
1. Reading data into memory 4 slices at a time.
2. Generating a cube(voxel) from four neighbors in two consecutive slices.
3. Determining the shape of the surface within the cube based on comparing the image intensity value at each of the eight vertices with the pre-selected surface intensity or threshold value [See Figure 5].
4. Using linear interpolation techniques to determine the surface-edge intersection for the required edges of the cube.

5. Employing central differences to calculate a unit vector for each vertex of the cube and then interpolating the normal to each triangle vertex.
6. Finally, outputting triangular polygons (3 vertices and the corresponding vertex normals)
7. Repeating this sequence of steps for all the slices in the volume.

Applying this volume visualization technique to the 3D SPECT data yields a triangulated polygonal mesh representing the structure of the myocardium [See Figure 6]. This mesh is further refined to smooth out the surface to assist in the subsequent analysis of the topology. It should be noted here that a 3D mesh is not the best visualization of this structure. Shading and animation enhance the visualization of the myocardium quite significantly. Such three-dimensional representation improves the orientation determination and interpretation capability of humans as well as of machine-based automatic systems. These individual components (polygons and their normals) of this structure are then employed to determine the orientation of the left-ventricular myocardium as explained in the following section.

4.1.4 Topological Goniometry

The final stage of this innovative scheme to determine the orientation of the left-ventricle involves analysis of the normals of each polygon in the topology. The normal of each polygon in the topology is backprojected (elongated) until it intersects with another polygon in the topology. Only those normal vectors with the point of intersection within a pre-determined distance, are chosen for the next stage of the process. The 3D midpoint of the line joining the base of the normal vector (\bar{n}) to the point of intersection is chosen as a candidate representing a point on or near the long-axis of the left ventricle. All such candidate points are collected. At this stage of the algorithm we have a 3D scatter of points on or near the "true" long-axis of the heart. See Figure 7 for a better illustration of this step.



Depending upon the object shape, a data fitting algorithm is now applied to estimate the pose of the 3D object, which represents the 3D medial axis of the object. At this stage we have two main options : (1) fit the 3D scatter of points to a straight line assuming that the overall shape of the myocardium is an ellipsoid or (2) fit a 3D curve to the 3D scatter. For evaluation purposes, we have constrained ourselves to a straight line fit of the 3D data. This allows us to compare the orientation of the LV as computed by the automated algorithm to that determined by the medical technicians. In our visualization of the LV orientation we present the 3D curve representation of the LV long-axis.

For finding a 3D straight-line fit, eigenvalue analysis is used. Let $p_i = (x_i, y_i, z_i)$ represent the coordinates of each mid-point selected in the last step. Principal moment analysis is performed to compute the predominant orientation of the 3D scatter of points. The eigenvector corresponding to the largest eigenvalue of the matrix A, as computed below, provides the desired principal directions. The matrix A is the covariance matrix of all points p_i and is computed as follows :

$$A = \left(\frac{1}{N}\right) \sum_{(i=1)}^N (p_i - \bar{p})^T (p_i - \bar{p})$$

where, N is the total number of candidates derived from the backprojection of normals and \bar{p} is defined as,

$$\bar{p} = \left(\frac{1}{N}\right) \sum_{i=1}^N p_i$$

Let $e = (e_x, e_y, e_z)$ be the eigenvector corresponding to the largest eigen value of A. Then,

$$\alpha = \tan^{-1}\left(\frac{e_y}{e_x}\right)$$

and,

$$\beta = \tan^{-1}\left(\frac{e_z}{\sqrt{e_x^2 + e_y^2}}\right)$$

These two angles provide the orientation of the LV myocardium.

5. RESULTS

The results in this ongoing research project are composed of two parts. The first direct result of this study is an automated technique to determine the patient-specific long-axis orientation of the left ventricular myocardium from SPECT data. The preliminary assessment of the automated algorithm has provided very encouraging results. A summary of these results is presented below. The second main accomplishment of this process is the ability to interactively visualize the three dimensional structure and orientation of the myocardium. This visualization significantly enhances the capability of determining and assessing the orientation of 3D objects within 3D data.

5.1 Orientation determination

The algorithm presented here to determine the LV orientation was applied to seven(7) normal and five(5) abnormal patients each of whom underwent rest and stress tests using Thallium²⁰¹ cardiac SPECT. The resultant information consists of a total of 24 3D datasets. For the same set of data, two medical technicians also determined the 2 angles α and β manually on a GE starcam 3000. The angles as reported by the automated routine were compared to the mean values of those reported by the medical technicians. Excellent agreement was observed between the angles computed by the automated algorithm and those determined by the two technicians manually (*See Table 1 below*). \bar{m}_1 was computed by averaging the absolute value of the dif-

Table 1: Error Analysis of the Automatic Orientation Determination Algorithm

Error Quantity	NORMAL PATIENTS		ABNORMAL PATIENTS	
	α	β	α	β
Mean ABS (\bar{m}_1)	4.58°	7.11°	6.92°	5.90°
Std. Dev. ($\bar{\sigma}_1$)	3.86°	5.49°	3.68°	6.36°

ference between the automatically computed angle and the mean of the angles reported by the two medical technicians over all the datasets. The same data was analyzed for computing the standard deviation $\bar{\sigma}_1$. The inter-observer differences were also recorded and are listed in *Table 2 below*. The mean absolute difference (\bar{m}_2) between the two observers for each of the angles in the normal and abnormal categories along with the standard deviation ($\bar{\sigma}_2$) is reported below.

Table 2: Inter-Observer Variability Data

	NORMAL PATIENTS		ABNORMAL PATIENTS	
	α	β	α	β
Mean ABS (\bar{m}_2)	3.41°	2.34°	4.58°	1.80°
Std. Dev. ($\bar{\sigma}_2$)	3.34°	1.32°	3.80°	2.61°

5.2 Visualization

The iso-surface rendition of the original 3D data at the optimal threshold value has yielded great insight into the structure and orientation of the left ventricular myocardium as shown in *Figure 8*. These surfaces were generated using the Marching Cubes Algorithm^{13,14,15,16} and visualized using the *Advanced Visualizer*© software from Wavefront Technologies on an SGI 4D/120/GTX workstation. Another visualization model was generated using ray-casting techniques on the same volume data, the results of which are presented in *Figure 9*. It should be pointed out that a static presentation of a volumetrically rendered model is not optimal for viewing; this limitation is apparent from *Figure 9*. This visualization, generated using the *Data Visualizer*© software from Wavefront Technologies, is enhanced through dynamic animation. Such volumetric representation and analysis provides a mechanism for visualizing 3D data both subjectively and objectively within an integrated and highly interactive framework.

Finally, the visualization of the orientation of the left ventricle and the determined long-axis is highlighted in *Figure 10*. The model of the LV myocardium consists of about 2000 triangular polygons and is rendered using Gouraud shading using a single light source and a transparent material. The transparent property of the material allows for an "in-depth" view of the myocardium and the determined long-axis. An animated sequence of a fly-through the myocardium along the long-axis yields a highly interesting and intuitively appealing visualization.

6. CONCLUSIONS AND FUTURE DIRECTIONS

In this paper, we have discussed an automated technique to determine the orientation of the left ventricle from 3D cardiac SPECT studies. In addition, the importance of visualizing this information is also emphasized. The algorithm described provides the long axis (medial axis) of the left ventricle. This information can be used further to reorient the 3D dataset and to provide the short-axis slices to more accurately visualize the myocardial perfusion distribution. As a natural extension of this project the authors intend to improve the user interface and integrate the visualization and orientation determination aspects of this tool. In the very near future we also plan to analyze gated SPECT data to analyze and visualize the changes in the structure of the left ventricle during the cardiac cycle. An extensive clinical evaluation of the accuracy of this methodology is currently underway and will analyze 50 Thallium²⁰¹ and 50 Tc^{99m} cardiac SPECT studies. It is also our aim to extend the applicability of this tool to other organs within the body (spinal cord, abdominal aorta etc.) and other non-medical uses.

7. ACKNOWLEDGEMENTS

This work was supported in part by grants R 29 LM04692 from the National Library of Medicine and 1 RO1 HL42052-01 from the National Institutes of Health..

8. REFERENCES

1. He ZX, Maublant JC, Cauvin JC, and Veyre A, "Reorientation of the Left Ventricular Long-Axis on Myocardial Transaxial Tomograms by a Linear Fitting Method," *The Journal of Nuclear Medicine*, vol. 32, no. 9, pp. 1794-1800, 1991.
2. DePuey EG, and Garcia EV, "Optimal Specificity of Thallium-201 SPECT through Recognition of Imaging Artifacts," *Journal of Nuclear Medicine*, vol. 30, pp. 441-9, 1989.
3. Cooke CD, Folks RD, Jones ME, Ezquerria NF, and Garcia EV, "Automatic Program for Determining the Long Axis of the Left Ventricular Myocardium used for Thallium-201 Tomographic Reconstruction," *Journal of Nuclear Medicine*, vol. 30, pp. 806, 1989.
4. He, ZX, "Automatic Reorientation of Left Ventricle Long Axis in Tl-201 SPECT Scans", *Proceedings of the European Association of Nuclear Medicine Congress*, Vienna, Austria, 1991.

5. Hoffman EJ, Huang SC, and Phelps ME, "Quantitation in Positron Emission Computed Tomography.: Effect of Object Size," *Journal of Computer Assisted Tomography*, vol. 3., pp. 299-308, 1979.
6. Cauvin JC, Maulblant JC, Boire JY, Zanca M, Bousquet V, and Veyre A, "Automatic Reorientation of the Myocardium in TL-201 SPECT," *Proceeding of the 38th Annual Meeting of the Society of Nuclear Medicine (SNM)* - Abstract No. 672, vol. 32, no. 5, pp. 1067, May 1991.
7. Blockland JAK, Vossepoel AM, Bakker AR, et. al, "Delineating Elliptical Objects with an Application to Cardiac Scintigrams," *IEEE Transactions on Nuclear Medicine*, vol. 1, pp. 57-66, 1987.
8. Garcia EV, DePuey SG, and Robbins W, "Emory Bullseye Protocol. Quantitative Thallium-201 Analysis of Stress and Delayed Myocardial Tomograms," Operating Instructions, Emory University School of Medicine, Atlanta, GA, May 1986.
9. Garcia EV, Train KV, Maddahi J, Prigent F, Friedman J, Areeda J, Waxman A, and Berman DS, "Quantification of Rotational Thallium-201 Myocardial Tomography," *Journal of Nuclear Medicine*, vol. 26, no. 1, pp. 17-26, 1985.
10. Ezquerria NF and Garcia EV, "Artificial Intelligence in Nuclear Medicine Imaging," *American Journal of Cardiac Imaging*, vol. 3, no. 2, pp. 130-141, 1989.
11. DePuey EG, Garcia EV, and Ezquerria NF, "Three-Dimensional Techniques and Artificial Intelligence in Thallium-201 Cardiac Imaging," *American Journal of Radiology*, vol. 152, pp. 1161-68, 1989.
12. Jain AK, "*Fundamentals of Digital Image Processing*," Englewood Cliffs, N.J., Prentice Hall, 1989 (Chapter 9)..
13. Cline HE, Dumoulin CL, Hart HR Jr., Lorenson WE, and Ludke S, "3D Reconstruction of the Brain from Magnetic Resonance Images Using a Connectivity Algorithm," *Magnetic Resonance Imaging*, vol. 5, pp. 345-352, 1987.
14. Cline HE, Lorenson WE, Ludke S, Crawford CR, and Teeter BC, "Two Algorithms for the Three-Dimensional Reconstruction of Tomograms," *Medical Physics*, vol. 15, no. 3, pp. 320-327, 1988.
15. Lorenson WE and Cline HE, "Marching Cubes : A High Resolution 3D Surface Construction Algorithm," *Computer Graphics*, vol. 21, no. 4, pp. 163-69, 1987.
16. Levoy M, Chairman, "Tutorial on Volume Visualization Algorithms," *First Conference on Visualization in Biomedical Computing*, May 22nd, 1990.

9. COLOR FIGURES

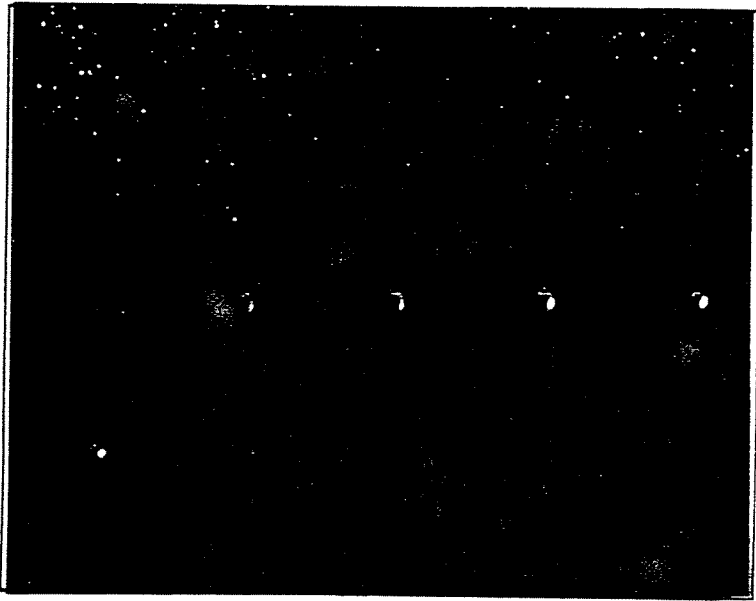


Figure 2. Transaxial tomographic slices

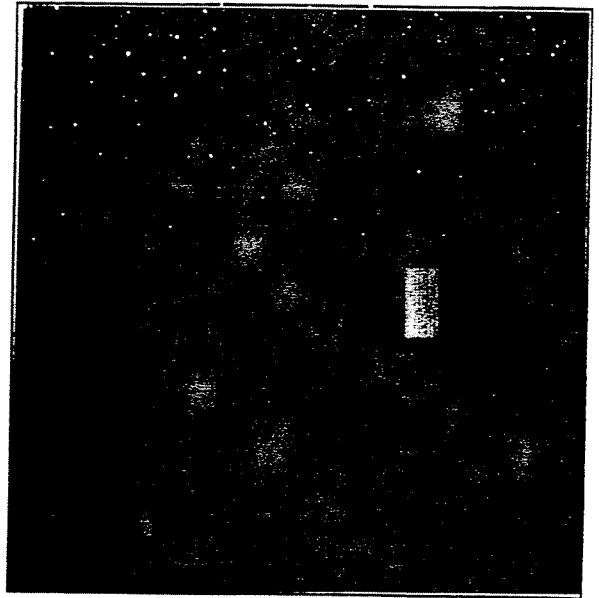


Figure 4. Filtered mid-ventricular slice (Magnified)

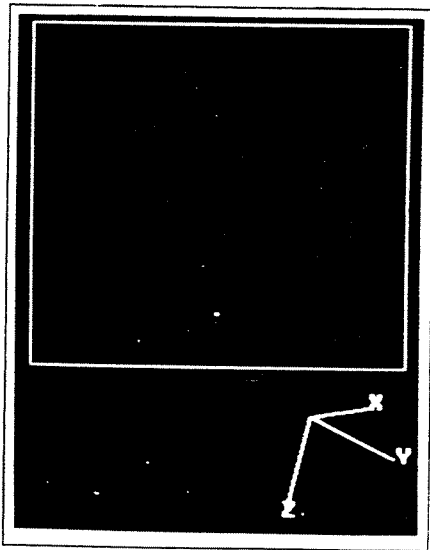


Figure 8.
Surface rendering of 3D myocardium.



Figure 9.
Volume visualization of 3D myocardium.

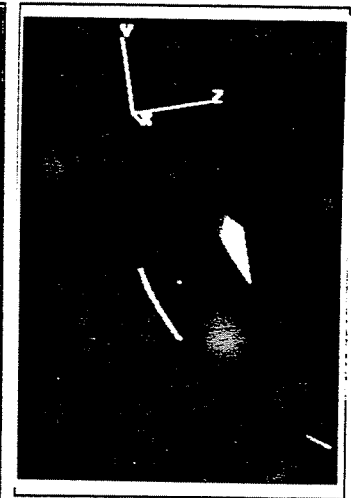


Figure 10.
Orientation visualization.